A short-lived oxidation event during the early Ediacaran and delayed oxygenation of the Proterozoic ocean

Bo Chen[1], Chunlin Hu[1,2], Benjamin J. W. Mills[3], Tianchen He[3,1], Morten B. Andersen[4], Xi Chen[5], Pengju Liu[6], Miao Lu[1], Robert J. Newton[3], Simon W. Poulton[3], Graham A. Shields[7], Maoyan Zhu[1,2]*

[1]State Key Laboratory of Palaeobiology and Stratigraphy & Center for Excellence in Life and Paleoenvironment, Nanjing Institute of Geology and Palaeontology, Chinese Academy of Sciences, Nanjing, China.

[2]College of Earth and Planetary Sciences, University of Chinese Academy of Sciences, Beijing, China.

[3]School of Earth and Environment, University of Leeds, Leeds, LS2 9JT, UK.

[4]School of Earth and Ocean Sciences, Cardiff University, Cardiff, CF10 3AT, UK.

[5]State Key Laboratory for Mineral Deposits Research, School of Earth Sciences and Engineering, Nanjing University, Nanjing, China.

[6]MNR Key Laboratory of Stratigraphy and Palaeontology, Institute of Geology, Chinese Academy of Geological Sciences, Beijing 100037, China

[7]Department of Earth Sciences, University College London, Gower Street, London, WC1E 6BT, UK.

*email: myzhu@nigpas.ac.cn

The Ediacaran Period was characterised by major carbon isotope perturbations. The most extreme of these, the ~570 Ma Shuram/DOUNCE (Doushantuo Negative Carbon isotope Excursion) anomaly, coincided with early radiations of benthic macrofauna linked to a temporary expansion in the extent of oxygenated seawater. Here we document an earlier negative excursion (the ~610 Ma WANCE (Weng'An Negative Carbon isotope Excursion) anomaly in the Yangtze Gorges area, South China, that reached equally extreme carbon isotope values and was associated with a similar degree of environmental perturbation. Specifically, new uranium isotope data evidence a significant,

but transient, shift towards more oxygenated conditions in tandem with decreasing carbon isotope values, while strontium and sulfur isotope data support an increase in continental weathering through the excursion. We utilize a biogeochemical modelling approach to demonstrate that the influx of such a weathering pulse into an organically-laden, largely anoxic ocean, fully reproduces each of these distinct isotopic trends. Our study directly supports the hypothesis that a large dissolved marine organic pool effectively buffered against widespread oxygenation of the marine environment through the Proterozoic Eon, and in doing so, substantially delayed the radiation of complex aerobic life on Earth.

Key words: DOM (Dissolved Organic Matter), carbon isotope perturbations, strontium isotopes, sulfur isotopes, uranium isotopes, Metazoans

1. Introduction

The Ediacaran-Cambrian transition was characterised by high amplitude $\delta^{13}C$ excursions in seawater (e.g. the 'Shuram/DOUNCE' isotope excursion), with negative values far below mantle input (~-6‰, V-PDB) (Burns and Matter, 1993; Grotzinger et al., 2011; Zhu et al., 2013; Shields et al., 2019). These extreme $\delta^{13}C$ anomalies are difficult to interpret using conventional carbon isotope mass balance, as they imply net consumption of oxygen by the carbon cycle (Lee et al., 2015), causing some to argue for a diagenetic or regional origin for these signals (Knauth and Kennedy 2009). It is, however, increasingly evident that Ediacaran-age negative $\delta^{13}C$ excursions are identical and correlative on a global scale (Xiao et al., 2016), reflecting a well-mixed primary seawater signal (Grotzinger et al., 2011; Lu et al., 2013).

Alternatively, it has been proposed that episodic oxidation of a large deep marine dissolved organic matter (DOM) reservoir released surplus ^{13}C-depleted carbon (around -30‰, V-PDB)

into the ambient dissolved inorganic carbon (DIC) reservoir at times during the Ediacaran Period, resulting in the observed highly-negative $\delta^{13}C$ anomalies (Rothman et al., 2003). However, this sequence of events has been questioned due to an apparent insufficient supply of oxidant (e.g. O_2, SO_4) to the Ediacaran ocean to sustain DOM oxidation over the multimillion-year timescales required (Bristow and Kennedy, 2008). Recently, however, Shields et al. (2019) used a biogeochemical model to show that a pulse of sulfate into the ocean from rapid continental gypsum dissolution could have supplied sufficient oxidizing capacity to produce the carbon isotope change evident in the ~570 Ma Shuram/DOUNCE event.

While this recent work has resolved the theoretical challenge to the DOM buffer hypothesis, direct geochemical evidence supporting this proposed chain of events is lacking, which is also the case with other super-negative carbon isotope excursions during the Neoproterozoic Era. Here, we present an integrated carbon, sulfur, uranium and strontium isotope study of the ~610 Ma WANCE anomaly in the Yangtze Gorges area, South China that provides the first direct geochemical evidence supporting the DOM buffer hypothesis. We then utilize the COPSE (Carbon, Oxygen, Phosphorus, Sulphur and Evolution) biogeochemical model to reproduce each of these distinct isotopic trends by setting up forcing parameters in line with the DOM buffer hypothesis. The robustness and universal implication of the DOM effect is further tested by investigating longer time-scale records for the Ediacaran and early Cambrian.

2. Geological setting and stratigraphy

Ediacaran strata, deposited in various settings ranging from shallow marine shelf to deep marine basin (Zhu et al., 2007) (Fig. 1), are well exposed over the Yangtze Platform of South China. The Yangtze Gorges area in western Hubei Province contains the most classic succession, comprising the Doushantuo Formation and overlying Dengying Formation, and has been intensively investigated over the past century (Zhu et al., 2007, 2013; Zhou et al., 2018)

(Fig. 1a, b, c). The Doushantuo Formation in the Yangtze Gorges area mainly comprises limestone with alternating organic-rich black shale and/or thinly bedded dolostone and phosphorite-chert nodules that were deposited in an offshore intra-shelf basin within the Yangtze platform (Zhu et al., 2013). Traditionally, the Doushantuo Formation is subdivided into four members (Members I–IV) based on their distinct lithologic characteristics in the Yangtze Gorges area (Zhou et al., 2018). Three major negative C-isotopic excursions known as EN1, (Ediacaran negative $\delta^{13}C$ excursion 1), (EN2, Ediacaran negative $\boldsymbol{\delta}^{13}C$ excursion 2) and (EN3, Ediacaran negative $\delta^{13}C$ excursion 3) were previously identified within the Doushantuo Formation and are widely used as key chemostratigraphic markers for both regional and global stratigraphic correlations (Zhou et al., 2018; McFadden et al., 2008). However, subsequent higher-resolution investigations found an additional $\delta^{13}C$ negative anomaly between EN1 and EN2 that is associated with a sequence boundary in the middle Doushantuo Formation deposited in the shallow shelf area of the Yangtze platform (Zhu et al., 2013; Gao et al., 2018, Fig. 2), indicating that there are at least four distinct negative carbon isotope excursions within the Doushantuo Formation, which, in ascending order, are named CANCE (CAP carbonate Negative Carbon isotope Excursion) (EN1), WANCE, BAINCE (Baiguoyuan Negative Carbon isotope Excursion (EN2) and DOUNCE (EN3) according to Zhou et al. (2018) and Zhu et al. (2013) (Fig 1c; Fig. 2).

The Nantuocun section is located along a roadcut above the southern bank of the Yangtze River ca. 3 km east of Sanduping town, at a site exactly opposite the well-known Liantuo Bridge on the northern bank of the Yangtze River. At this locality, the Doushantuo Formation outcrops as a basal cap carbonate (Member I) with overlying black shales followed by a ca. 40 meter-thick carbonate succession (lower part of Member II) dominated by dolostone and argillaceous dolostone with chert nodules (Fig. 1d; Fig. S1**)**. Abundant acritarch fossils were recovered in the chert nodules, including *Tianzhushania spinosa, Appendisphaera grandis, Estrella greyae,*

Estrella recta, *Estrella sp.*, *Dicrospinasphaera improcera*, *Distosphaera speciose*, *Ericiasphaera magna*, *Membranosphaera Formosa* and *Mengeosphaera lunula*. Biostratigraphic correlation of the acritarch assemblage confirms that the study interval of the Nantuocun section can readily be assigned to Member II of the Doushantuo Formation (Liu and Moczydłowska, 2019) (Fig. 1d), in line with independent correlation by means of litho- and carbon isotope stratigraphy (Fig. 1d). Based on the integrated correlation above, the extreme negative $\delta^{13}C_{carb}$ excursion observed in the Nantuocun section cannot be assigned to the DOUNCE anomaly, which is known from members 3 and 4 of the Doushantuo Formation only, and so is proposed to be time equivalent to the WANCE event reported from the middle part of Member II that was dated to 609±5 Ma by the zircon SIMS U-Pb method (Zhou et al., 2017).

The lower and upper boundaries of the Doushantuo Formation in the Yangtze Gorges area are well constrained to ca. 635 Ma and ca. 551 Ma, respectively, by high precision U-Pb zircon ages(Condon et al., 2005). However, high-precision radiometric ages are rare within the formation, hampering the subdivision and global correlation of Doushantuo strata as well as precise constraints on the extreme carbon cycle perturbations observed in this formation. However, cyclostratigraphy has been increasingly utilized to constrain the timing and duration of Ediacaran geochemical and/or extreme climatic events (Sui et al., 2018). For examples, Sui et al. (2018) identified 27 long-eccentricity (405 kyr) cycles from ca. 22.3 m strata in the lower Doushantuo Formation at the Jiulongwan section of the Yangtze Gorges area about 7 km from the Nantuocun section, suggesting an average sediment accumulation rate (SAR) of 1.95 m/Ma for the Doushantuo Members II. Based on this suggestion, the three meters of strata that record the WANCE event observed at Nantuocun section are estimated to have accumulated within about 1.5 Myr.

3. Methods

3.1 Carbonate carbon and oxygen isotopes

Carbonate powders were drilled from freshly cut rock slab surfaces using a micro-drill for carbon and oxygen isotope analyses. Fine-grained micrites were preferentially selected. Powders were reacted with 100% phosphoric acid at 70°C and analyzed for carbon and oxygen isotopes using a Kiel IV device connected to a Finnigan MAT 253 mass spectrometer at the Nanjing Institute of Geology and Palaeontology. Reproducibility was better than ±0.03‰ and ±0.08‰ (1s.d.) for carbon and oxygen isotopes, respectively. All analyses were calibrated to the Chinese National Standard (GBW-04405), an Ordovician carbonate from a site near Beijing, with a $\delta^{13}C$ value of 0.57‰ and $\delta^{18}O$ value of −8.49‰. All data are given in per mil (‰) relative to V-PDB.

3.2 Organic carbon isotopes

For organic carbon isotope analyses, about 5 g of powdered carbonate was reacted with concentrated HCl, followed by repeat checks using drops of HCl to confirm complete decarbonization. The residues were then repeatedly washed with deionized water until the pH reached near neutral, and samples were dried in an oven. The residues were then wrapped into tin capsules for organic carbon isotope and total organic carbon (TOC) measurements, which were performed with a Flash EA 2000 elemental analyser connected online to a Thermo Finnigan Delta V Plus mass spectrometer. All carbon isotope values are reported in the conventional δ-notation in permil relative to V-PDB. Reproducibility of the analyses was checked by replicate analyses of laboratory standards black carbon (GBW04407) and Urea (IVA33802174). Reproducibility was better than 0.2‰ for $^{13}C_{org,}$ and 0.02 wt% for TOC.

3.3 Carbonate-associated sulfate (CAS) and pyrite sulfur isotopes

This study used a state-of-the-art CAS extraction method (He et al., 2020) and extraction work was carried out in the Cohen Geochemistry laboratory, University of Leeds. For bulk carbonate samples, 8-10 g of fine powder was first bleached in 6% NaOCl for 48 hours to remove oxidize organic sulfur and metastable sulfide minerals, followed by a five times wash in 10% NaCl solution for 24 hours to remove the non-CAS sulfur-bearing compounds or easily soluble sulfate. Pre-bleached carbonate residues were then treated with 6 M HCl to extract CAS. CAS was collected by precipitation as barium sulfate. We also measured sulfur concentrations in the extracted solution using a Thermo Fisher iCAP 7400 Radial Inductively Coupled Plasma Optical Emission 280 Spectrometer (ICP-OES) in the Cohen Geochemistry laboratory, University of Leeds. Pyrite extractions were performed following an HCl digestion and chromous chloride distillation method (Canfield et al., 1986). The barium sulfate precipitates from the CAS extraction and silver sulfide from the pyrite extraction were weighed into tin cups, which were combusted to yield SO_2. $\delta^{34}S$ values were determined using a Flash EA 2000 elemental analyzer coupled to a Delta-Advantage mass spectrometer at the NIGPAS. All samples and standards are reported relative to the Vienna Canon Diablo Troilite (V-CDT) standard, with an analytical reproducibility of 0.3‰ calculated from replicate analyses of IAEA standards (NBS-127, IAEA-1, IAEA-SO-6).

3.4 Elemental concentrations

Approximate 50 mg of sample powder was weighed and dissolved in 3 mL of distilled 1 M acetic acid and left to dissolve overnight. The solutions were centrifuged, and the supernatant transferred to another breaker. The residues were rinsed three times using ultrapure water and the solutions were added to the previous supernatant. The leachates were converted to nitric acid medium, which was then used for elemental analysis. Element analysis was carried out at the element laboratory in the NIGPAS. Trace and REE concentrations were determined using

an Agilent 7700A inductively coupled plasma mass spectrometer (ICP-MS) with analytical precision better than ±2%. Major elements were measured using an Agilent 710 ICP-OES with analytical precision better than ±5%.

3.5 Strontium isotopes

The samples having lower Mn/Sr ratios (<2) were selected for strontium isotope analyses. The carbonate powders were mixed with 0.5 N acetic acid, and the solution was then centrifuged at 3300 rpm for 10 min, after which the supernatant was dried down on a hotplate and redissolved in 1.5 ml of 1.5 N HCl before ion exchange purification. A Biorad AG50W-X8 cation exchange column was used to separate Sr from other elements. The diluted solutions (50 ppb Sr) were introduced into a Nu Instruments *Nu Plasma II* MC-ICP-MS (Wrexham, Wales, UK) through a Teledyne Cetac Technologies *Aridus II* desolvating nebulizer system (Omaha, Nebraska, USA) for $^{87}Sr/^{86}Sr$ analysis. Raw data for Sr isotopic ratios were internally corrected for mass fractionation by normalizing to $^{86}Sr/^{88}Sr = 0.1194$ with exponential law. International isotopic standards NIST SRM 987 were periodically analyzed to correct instrumental drift. Standard sample NBS 987 was measured every three samples, yielding an average value of 0.710240 (σ= ±0.000045, n=17). The standard error for Sr isotope analysis was between 0.000004-0.000008, All results were corrected to NIST 987 as 0.710248. Sr isotope measurements were carried out at Nanjing FocuMS Technology Co. Ltd.

3.6 Uranium isotopes

For carbonate-associated uranium isotopes ($^{238}U/^{235}U$ reported as $\delta^{238}U_{CAU}$) ananysis, between 0.2 to 1 g of carbonate powder was digested using excess 1 N HCl at room temperature for several hours, until no further effervescence was observed. The leachate was separated from any residue and spiked with the IRMM3636 ^{236}U-^{233}U double spike. Uranium purification was

performed using a double-stage TRU and U-Teva column chemistry (Andersen et al., 2015). Full uranium recovery (>95%) and practically matrix-free samples were obtained with this method, with total procedural U chemistry blank <20 pg. The analyses were carried out on a Nu Instruments *Nu Plasma II* MC-ICP-MS (Wrexham, Wales, UK) through Teledyne Cetac Technologies *Aridus II* desolvating nebulizer system (Omaha, Nebraska, USA) at CELTIC, Cardiff University. The U isotope measurements were conducted in 0.3 N HNO_3 + 0.02 N HF at low mass resolution (M/M ~400). The data were collected in static mode for all the isotopes of interest (^{232}Th, ^{233}U, ^{234}U, ^{235}U, ^{236}U, ^{238}U) in Faraday cups fitted with 11^{11} Ω resistors, generally following the set-up in Stirling et al. (2007). General U transmission efficiencies were ~1% and measurements were conducted using typical ^{238}U ion beams of ~4 x 10^{-10} amps with data integration over a 60 x 5 seconds period. Washout in between samples consisted of a sequence of ~3 min 0.3 N HNO_3, ~3 min 0.3 N HNO_3-0.01 N HF, and ~2 min of 0.3 N HNO_3. The final wash also served as an on-peak blank measurement and was subtracted from the succeeding sample measurement. Corrections of ^{238}U and ^{235}U impurities in IRMM3636, tailing, H^+ formation and mass bias corrections followed Andersen et al. (2014, 2015, 2016). The accuracy of the set-up was first tested by measuring secondary standards bracketed and normalized to the CRM 145 standard spiked, and measured in a similar manner to the unknowns. The $^{238}U/^{235}U$ ratios are reported as $\delta^{238}U$ (= 1.000×[($^{238}U/^{235}U$) Sample/ ($^{238}U/^{235}U$) $_{CRM\text{-}145}$ − 1]). Values are reported relative to the NBL CRM-145 natural U standard. The internal precision on measured $\delta^{238}U$ values are better than ±0.05‰ (2 standard error) for all samples. The external reproducibility of $\delta^{238}U$ for the in-house CZ-1 gave $\delta^{238}U$ of -0.04 ± 0.07‰ (2 sd, 11 measurements) in good agreement with previously reported values (e.g. Andersen et al., 2014, 2015, 2016; Stirling et al., 2007), while duplicate measurements of HU-1 (-0.56 ± 0.06 and -0.58 ± 0.05, 2 standard error) are also in very good agreement with previously reported results (Hiess et al., 2012).

4. Results

We present strontium, uranium and sulfur isotope analyses through a newly identified negative $\delta^{13}C_{carb}$ excursion, which exhibits a sharp fall from +6‰ to a nadir of -10‰, followed by a sharp recovery within an ~3 meter interval of the lower Doushantuo Formation (early Ediacaran) in the Yangtze Gorges area, South China (Fig. 3, Fig. S2). Integrated stratigraphic data suggest that the negative $\delta^{13}C_{carb}$ excursion is correlative to the WANCE excursion and therefore predates the well-known 'Shuram/DOUNCE' event by about 30 Myr (see Fig. 1 and 2).

An evaluation of possible diagenetic alteration of carbon, strontium, uranium and sulfur isotope data based on geochemical crossplots, petrographic and mineralogical observations, and regional stratigraphic correlations suggests that this event archives a primary seawater geochemical perturbation that was widespread (see more details in the Supplementary Information), at least extending across the Yangtze Gorges area in South China (Fig. 2)

$\delta^{34}S_{CAS}$ values from the Nantuocun section show a significant increase from +40‰ to +60‰ beneath the WANCE followed by a sharp decline to +30‰ (V-CDT) alongside the falling limb of the WANCE (Fig. 3), accompanied by ~10‰ (V-CDT) decrease in pyrite sulfur isotope values (δ^{34}Spyr) (Fig. 3). Both $\delta^{34}S_{CAS}$ and δ^{34}Spyr values are relatively invariant above the WANCE. The $\delta^{238}U$ values show relatively stable values around -0.55 ‰ below the WANCE followed by a sharp rise to -0.2‰, parallel with the falling limb of the WANCE, an abrupt decrease to -0.86‰ as $\delta^{13}C$ values reach their nadir, and then by relatively invariant values around -0.55‰. Strontium isotope ($^{87}Sr/^{86}Sr$) data from the section reveal a pronounced increase from ~0.7078 to ~0.7084, succeeded by a decrease to ~0.7081, following which there was no significant change. The $^{87}Sr/^{86}Sr$ increase initiated prior to the WANCE, whereas the decline coincides with the nadir of $\delta^{13}C_{carb}$ **(**Fig. 3**).**

5. Discussion

5.1 A short-lived oxidation event during the early Ediacaran

As shown in Figure 4, seawater sulfate ($\delta^{34}S_{CAS}$) and pyrite ($\delta^{34}S_{pyr}$) sulfur isotope values fell by ~30‰ and ~10‰ (V-CDT), respectively, alongside the falling limb of the $\delta^{13}C_{carb}$ excursion. As in the later Shuram excursion, the substantial long-term decrease in $\delta^{34}S$ may indicate a large pulse of sulfate input into a sulfate-poor ocean (Shi et al., 2018), effectively resetting the isotope composition closer to that of the weathered gypsum (and pyrite), which was likely no higher than +15‰ (Shields et al., 2019). The extreme-negative $\delta^{13}C$ excursion is consistent with oxidation of DOM, and the presence of a brief oxygenation event is further supported by evidence from carbonate-associated uranium isotope values, which are utilized as a proxy for oceanic $\delta^{238}U$. This record exhibits an abrupt rise in $\delta^{238}U_{CAU}$ just before the nadir in the C isotope record, from initial values below, to values above, modern oxygenated seawater (~-0.4‰) (Fig. 3). Rising $\delta^{238}U_{CAU}$ values are associated with reduced rates of sequestration of isotopically heavy uranium under anoxic conditions globally, which increases $\delta^{238}U$ in the ocean (Andersen et al., 2014). Thus, the increasing $\delta^{238}U_{CAU}$ trend associated with WANCE likely documents a rapid expansion of oxic seafloor area in the early Ediacaran ocean.

The onset of the WANCE event is also marked by an increase in seawater $^{87}Sr/^{86}Sr$, alongside a rise in $\delta^{34}S_{CAS}$ towards its highest value in the geological record (~60‰) (Fike et al., 2015) (Fig. 3). The combination of rising seawater $^{87}Sr/^{86}Sr$ and sulfate $\delta^{34}S$, alongside much lower pyrite $\delta^{34}S$, suggests that enhanced weathering, likely due to tectonic uplift associated with the amalgamation of Gondwana (Campbell and Squire, 2010), may have exhumed major basin-scale evaporite previously deposited during the Tonian Period (Turner and Bekker, 2016) or earlier, resulting in high pyrite burial rates. This is because a large isotopic fractionation between sulfate and pyrite ($\Delta\delta_{CAS\text{-}pyr}$ > ~35‰) (Fig. 3) is only compatible with abundant dissolved sulfate (Habicht and Canfield, 2018), while pyrite burial is related through organic

production to weathering input of nutrients as well as sulfate. By contrast, the sharp drop in $\Delta\delta_{CAS\text{-}pyr}$ to significantly lower values (~20‰) around the lowest point of the negative $\delta^{13}C_{carb}$ excursion, may signal a return to lower oceanic sulfate concentrations and reduced rates of pyrite burial, alongside greater oxidation of continental pyrite (Fig.3).

5.2 Reproducing the oxidation event in the COPSE biogeochemical model

Our combined carbon, sulfate, strontium and uranium isotope data suggest that the WANCE represents a marine oxygenation event driven by enhanced weathering input of sulfate, with the extent of oxygenation mediated by oxidation of a large marine DOM reservoir. In order to quantitatively test this hypothesis, we employ the COPSE biogeochemical model (Bergman et al., 2004), which computes the major long-term fluxes of carbon, oxygen, phosphorus, nitrogen and sulfur through Earth's hydrosphere and crust. COPSE is a 'forwards' model in which processes are driven by a set of evolving boundary conditions (forcing factors) and internal dynamics, including a nutrient-driven biosphere (See Supplementary Information for full model description). We use the latest COPSE model revision (Tostevin and Mills, 2020) which includes forcing information for the Ediacaran Period (Williams et al., 2019) and simplified DOM reservoir dynamics (Shields et al., 2019). See bjwmills.com for model code.

We run COPSE through the Ediacaran Period and impose a sulfate input event at the time of the observed negative carbon isotope excursion to examine the dynamics of an oxygenation event at this time. In order to make the model most applicable to the short time interval being tested we make the following alterations:

1. COPSE has very strong negative feedbacks on marine sulfate concentrations and is unable to reproduce the low sulfate ocean expected for the Ediacaran. To begin with low sulfate concentration, we increase the power of the sulfate sinks by factor $PYR_{mod} = GYP_{mod} =$

10. This allows the model to enter the Ediacaran Period with $[SO_4] \approx 1$ mM.

2. To match the background pre-event carbon and sulfur isotope records we set the isotopic compositions of inputs from carbonates, organic carbon, pyrite and gypsum to be 5‰, -20‰, 5‰ and 50‰, respectively. This is based on the observed composition of seawater before the event. Similarly to match the strontium isotope record we set the Rb/Sr ratio of felsic lithologies in the model to 0.29 (from 0.26 in the original model).

To drive the oxygenation event in the model we impose an input of sulfate from the weathering of continental evaporites and pyrites at 610.5 Ma, coinciding with the beginning of the strontium and carbon isotope excursions. Specifically, the model forcing is:

$$GYP_{input} = [-1000 - 610.5 - 610.4 - 609.5 - 609.4\ 0], [0\ 0\ GYP_{ramp}\ GYP_{Ramp}\ 0\ 0]$$

$$PYR_{input} = [-1000 - 610.5 - 610.4\ 0], [0\ 0\ PYR_{ramp}\ PYR_{Ramp}]$$

where the first vector is time in millions of years before present, and the second is the additional weathering flux. We take $PYR_{Ramp} = 1$ (which corresponds to a doubling) and $GYP_{Ramp} = 5 - 15$. It is assumed that an uplift-weathering event will result in rapid dissolution of gypsum (Shields et al., 2019), whereas weathering of pyrite will be sustained at lower levels over a longer period since it is a sink for O_2. The magnitude of the weathering rate increase is consistent with previous estimates for global evaporite dissolution (Shields et al., 2019; Wortmann and Paytan, 2012), and requires a total gypsum supply of around 1-2 x 10^{19} mol S, which is well within plausible bounds. These additional inputs of sulfur are assumed to be buried almost completely as pyrite (following Shields et al., 2019), although we raise the pyrite burial fraction to 95% (from 80% in that paper) in order to explore the ability of the model to match the extreme positive $\delta^{34}S$ values.

Our model seawater isotope ratio results are shown in Figure 4, and are compared directly to our strontium, sulfur and carbon isotope data. The COPSE model does not include a uranium reservoir and cannot accurately predict the behaviour of this elemental cycle because it has a single 'atmosphere-ocean' reservoir for oxygen, with no explicit treatment of marine versus atmospheric oxygenation. Instead, marine anoxia in COPSE is represented by a variable called *anox*, which represents the balance between atmosphere/ocean O_2 availability and the size of the marine phosphorus reservoir (i.e. O_2 is supplied to the ocean by the atmosphere and is utilized during remineralization). DOM oxidation is assumed to begin once *anox* crosses a certain threshold (Shields et al., 2019). In order to examine O_2 production in the model relative to the marine $\delta^{238}U$ record, we qualitatively compare the U isotope data to variations in the model atmosphere-ocean O_2 reservoir (Fig. 5), accepting that changes in $\delta^{238}U$ might occur much more rapidly than changes to the overall surface O_2 reservoir, due to oxygen-nutrient feedbacks and changes to the area of oxic seafloor (e.g. Alcott et al., 2019).

In our model scenario, the rapid increase in sulfate input from gypsum weathering leads to increased rates of microbial sulfate reduction and pyrite burial, resulting in a steady rise in O_2 availability (Fig. 5). After around 300 kyrs, the marine anoxia threshold is crossed (when O_2 supply from the atmosphere is sufficient; $O_2 \approx 1 \times 10^{19}$ mol) and the DOM reservoir starts to be remineralised. This drives the $\delta^{13}C$ composition of marine DIC to very low levels (Fig. 4), while also placing a break on further oxygenation. Overall atmosphere-ocean O_2 content continues to rise at a reduced rate (Fig. 5) until the sulfate input abates and the system quickly returns to the background state. Here, O_2 is quickly consumed by the DOM reservoir until the assumed anoxia threshold in the model is crossed again, after which DOM oxidation ceases and $\delta^{13}C$ returns to the initial value. Figures 4 and 5 confirm that the timescale and magnitude of the perturbation and recovery of carbonate $\delta^{13}C$ and $\delta^{238}U$ values are consistent with a sulfate

input event under a DOM buffer. One aspect we cannot investigate with the COPSE model is the relatively constant $\delta^{13}C_{org}$ composition across the WANCE. This 'decoupled' behavior of the organic and inorganic carbon pools has been linked to the presence of a large DOM reservoir before (Rothman et al., 2003), but COPSE cannot recreate it because organic matter is not considered as a dynamic reservoir, and sedimentary C_{org} can only be buried directly from the DIC pool.

In addition to the carbon-oxygen systematics, the model also produces a reasonable fit to strontium and sulfur isotope values across the WANCE event (Fig. 4). Strontium $^{87}Sr/^{86}Sr$ ratios rise during the gypsum dissolution event in the model because the rapid remineralization of DOM increases atmospheric CO_2 and global temperature, thus delivering more radiogenic Sr to the ocean. Sr ratios in the model then level off when the weathering event abates, although not to the same degree shown by the data. The measured sulfur isotope ratios show the most complex pattern over this event, rising initially but then falling dramatically around the time of the C isotope reversal (Fig. 4). This behaviour is replicated to some degree by the model. Here, the initial rise in $\delta^{34}S$ is driven by exceptionally high pyrite burial rates as sulfate is delivered to productive margins underlain by dominantly anoxic waters and sediments. When the sulfate supply shuts down, the $\delta^{34}S$ ratio of seawater is reduced as pyrite burial is curtailed, and dips below the pre-event value due to the low $\delta^{34}S$ values of the evaporite sulfur influx (15 ‰).

Although there are some discrepancies between the model and our dataset, these are relatively minor and the overall level of qualitative and quantitative agreement over four distinct geochemical proxies is strong. We therefore conclude that there was a substantial influx of oxidant to the atmosphere and oceans during the WANCE, but that marine oxygenation was ultimately prevented by a large reservoir of DOM. The total consumption of DOM in this case

379 is 1-2 x 10^{19} mols of carbon, requiring an equal amount of molecular oxygen, equivalent to
380 around half of the present-day atmosphere-ocean reservoir.
381
382 **5.3 Delayed oxygenation of the Proterozoic ocean and implications for the rise of**
383 **metazoans**
384 Similar extreme carbon cycle perturbations are observed in later Ediacaran times, most
385 notably, the 'Shuram/DOUNCE' of the middle Ediacaran (eg. Lu et al., 2013) . The Shuram
386 event is thought to have been a longer oxygenation event that coupled enhanced evaporite
387 weathering and DOM oxidation (Shi et al., 2018; Fike et al., 2006; McFadden et al., 2008),
388 suggesting that episodic pulsed oxidant (sulfate) input was a uniform driver behind these
389 extreme negative carbon isotope excursions of the Ediacaran Period. These, in turn, governed
390 the redox status of the Ediacaran ocean, as exemplified by dramatic oscillations comprising
391 multiple transient oxygenation events punctuated by intervals of more widespread marine
392 anoxia (Sahoo et al., 2012) (Fig. 6), while brief oxygenation during the WANCE event
393 represents an earlier excursion to a more oxygenated state.
394 Significantly, the episodic expansion of oxygenated seafloor area through the Ediacaran
395 Period may have provided variable habitable space and ecological niches for the development
396 of complex macro-eukaryotes and primitive metazoans (e.g. the Weng'an and Lantian biotas in
397 the lower Doushantuo Formation (Xiao et al., 1998; Yuan et al., 2011; Yin et al., 2015),
398 However, biological innovations in connection with these brief oxygenation events may have
399 been discrete and interrupted by evolutionary lags or extinctions due to episodic reversals back
400 to widespread marine anoxia (Zhu et al., 2013; Wood et al., 2019). Innovations requiring higher
401 oxygen demand (e.g. motility, biomineralisation, predation; Fig. 6) appear to have emerged
402 only after the mid-late Ediacaran, with diversification during the early Cambrian radiations
403 (Wood et al., 2019). These opportunistic radiations of aerobic life forms may have promoted
404 subsequent innovations and feedbacks that eventually prevented a return to the prior turbid state

(Butterfield et al., 2009; Lenton et al., 2014), enabling ocean oxygenation to reach near modern levels by the early Cambrian (Chen et al., 2015).

6. Conclusions

Integrated carbon, sulfur, uranium and strontium isotope analyses of the ~610 Ma WANCE anomaly in the Yangtze Gorges area, South China, document a brief shift towards more oxygenated conditions. This oxygenation is consistent with surplus oxidant (SO_4) supply from increased continental weathering that resulted in a sharp decline in carbonate $\delta^{13}C$ to far below mantle values (nadir ~-10‰). Once the available oxidant was exhausted, the ocean rapidly returned to anoxia, accompanied by a $\delta^{13}C$ recovery to positive values. This pattern is consistent with observations from the ~570 Ma Shuram/DOUNCE anomaly, suggesting that surplus oxidant input may have been a uniform driver behind the extreme negative carbon isotope excursions of the Ediacaran Period.

The dynamic balance between ocean redox state and oxidant supply strongly supports the hypothesis that a marine DOM pool effectively suppressed oxygenation of the marine environment throughout most of the Proterozoic, placing a major constraint on the persistence of Proterozoic ocean anoxia. Significantly, this brief oxygenation event may signal the onset of a new transitional phase characterized by the pulsed destruction of a large oceanic dissolved organic carbon reservoir, which ultimately facilitated the higher marine oxygen concentrations required by more complex ecosystems.

References

Alcott, L.J., Mills, B.J.W., Poulton, S.W., 2019. Stepwise Earth oxygenation is an inherent property of global biogeochemical cycling. Science 366, 1333-1337.

Andersen, M.B., Romaniello, S., Vance, D., Little, S.H., Herdman, R., Lyons, T.W., 2014. A modern framework for the interpretation of 238U/235U in studies of ancient ocean redox. Earth and Planetary Science Letters 400, 184-194.

Andersen, M. B., Elliott, T., Freymuth, H., Sims, W. W. K., Niu Y., Kelley K. A., 2015. The terrestrial uranium isotope cycle. Nature 517, 356-359,.

Andersen, M. B., Vancea, D., Morford, J.L., Bura-Nakića, E., Breitenbach, S. F. M., Och, L., 2016. Closing in on the marine $^{238}U/^{235}U$ budget. Chemical Geology 420, 11-22,.

Andersen, M. B., Stirling C. H., Weyer S., 2017. Uranium Isotope Fractionation. Reviews in Mineralogy and Geochemistry 82, 799-850.

Burns, S. J. and Matter, A., 1993. Carbon isotopic record of the latest Proterozoic from Oman. Eclogae Geologicae Helvetiae 86, 595–607.

Berner, R. A., 1991. A model for atmospheric CO_2 over Phanerozoic time. American Journal of Science 291, 339-376,

Bergman, N. M., Lenton, T. M. & Watson, A. J., 2004. COPSE: A new model of biogeochemical cycling over Phanerozoic time. American Journal of Science 304, 397-437.

Bristow, T.F., Kennedy, M. J., 2008. Carbon isotope excursions and the oxidant budget of the Ediacaran atmosphere and ocean. Geology 36, 863.

Butterfield, N. J., 2009. Oxygen, animals and oceanic ventilation: an alternative view. Geobiology 7, 1–7.

Campbell, I.H and Squire R.J. 2010. The mountains that triggered the late neoproterozoic increase in oxygen: the second great oxidation event. Geochimica et Cosmochimica Acta, 74, 4187-4206.

Canfield, D. E., Raiswell,R., Westrich J. T., Reaves, C. M., Berner R. A., 1986. The use of chromium reduction in the analysis of reduced inorganic sulfur in sediments and shales. Chemical geology 54, 149-155.

Chen, X., Ling, H.F., Vance, D., Shields-Zhou, G.A., Zhu, M., Poulton, S.W., Och, L.M., Jiang, S.Y., Li, D., Cremonese, L., Archer, C., 2015. Rise to modern levels of ocean oxygenation coincided with the Cambrian radiation of animals. Nature Communications. 6, 7142.

Condon, D., Zhu, M., Bowring, S., Wang, W., Yang, A., Jin, Y., 2005. U-Pb ages from the neoproterozoic Doushantuo Formation, China. Science 308, 95-98.

Dahl, T. W., Connelly, J. N., Li, D., Kouchinsky, A., Gill, B. C., Porter, S., Maloof, A. C., Bizzarro, M., 2019. Atmosphere–ocean oxygen and productivity dynamics during early animal radiations. Proceedings of the National Academy of Sciences 116, 19352-19361.

Fike, D.A., Grotzinger, J.P., Pratt, L.M., Summons, R.E., 2006. Oxidation of the Ediacaran ocean. Nature 444, 744-747.

Fike, D. A., Bradley A. S., Rose C. V., 2015 Rethinking the ancient sulfur cycle. Annual Review of Earth and Planetary Sciences 43, 593-622.

Gao, Y., Zhang, X., Zhang G., Chen K., Shen, Y., 2018. Ediacaran negative C-isotopic excursions associated with phosphogenic events: Evidence from South China. Precambrian Research 307, 218-228.

Grotzinger, J.P., Fike, D.A., Fischer, W.W., 2011. Enigmatic origin of the largest-known carbon isotope excursion in Earth's history. Nature Geoscience 4, 285-292.

Habicht, K. S. & Canfield, D. E., 1996. Sulphur isotope fractionation in modern microbial mats and the evolution of the sulphur cycle. Nature 382, 342-343.

He, T., Dal Corso, J., Newton, R.J., Wignall, P.B., Mills, B.J.W., Todaro, S., Di Stefano, P., Turner, E.C., Jamieson, R.A., Randazzo, V., Rigo, M., Jones, R.E., Dunhill, A.M., 2020. An enormous sulfur isotope excursion indicates marine anoxia during the end-Triassic mass extinction. Science Advances 6, eabb6704.

Hiess, J., Condon, D. J., McLean N., Noble S. R., 2012 $^{238}U/^{235}U$ Systematics in Terrestrial Uranium-Bearing Minerals. Science 335, 1610-1614.

Knauth, L.P., Kennedy, M.J., 2009. The late Precambrian greening of the Earth. Nature 460, 728-732.

Lee, C., Love, G.D., Fischer, W.W., Grotzinger, J.P., Halverson, G.P., 2015. Marine organic matter cycling during the Ediacaran Shuram excursion. Geology, G37236.37231.

Lenton, T. M. & Watson, A. J. Redfield revisited: 1. Regulation of nitrate, phosphate, and oxygen in the ocean. Global Biogeochemical Cycles 14, 225-248, (2000).

Lenton, T.M., Boyle, R.A., Poulton, S.W., Shields-Zhou, G.A., Butterfield, N.J., 2014. Co-evolution of eukaryotes and ocean oxygenation in the Neoproterozoic era. Nature Geoscience 7, 257-265.

Li, D., Ling, H., Shields-Zhou, G. A., Chen, X., Cremonese, L., Och, L., Thirlwall, M., Manning, C. J., 2013 Carbon and strontium isotope evolution of seawater across the Ediacaran–Cambrian transition: Evidence from the Xiaotan section, NE Yunnan, South China. Precambrian Research 225, 128-147,

Liu, P. and Moczydłowska. M. 2019. Ediacaran microfossils from the Doushantuo Formation chert nodules in the Yangtze Gorges area, South China, and new biozones *in Fossils and Strata Series* 65, 1-172.

Lu, M., Zhu, M., Zhang, J., Shields-Zhou, G., Li, G., Zhao, F., Zhao, X., Zhao, M., 2013. The DOUNCE event at the top of the Ediacaran Doushantuo Formation, South China: Broad stratigraphic occurrence and non-diagenetic origin. Precambrian Research 225, 86-109.

Maloof, A. C., Porter, S. M., Moore, J. L., Dudás, F. Ö., Bowring, S. A., Higgins, J. A., Fike, D. A., Eddy, M. P., 2010. The earliest Cambrian record of animals and ocean geochemical change. GSA Bulletin 122, 1731-1774.

McFadden, K.A., Huang, J., Chu, X., Jiang, G., Kaufman, A.J., Zhou, C., Yuan, X., Xiao, S., 2008. Pulsed oxidation and biological evolution in the Ediacaran Doushantuo Formation. Proceedings of the National Academy of Sciences 105, 3197-3202.

Rothman, D. H., Hayes, J. M. Summons, R. E., 2003 Dynamics of the Neoproterozoic carbon cycle. Proceedings of the National Academy of Sciences 100, 8124-8129,.

Sahoo, S.K., Planavsky, N. J., Kendall, B., Wang, X ., Shi, X., Scott, C., Anbar, A.D., Lyons, T.W., Jiang, G., 2012. Ocean oxygenation in the wake of the Marinoan glaciation. Nature 489, 546.

Sawaki, Y., Ohno, T., Tahata, M., Komiya, T., Hirata, T., Maruyama, S., Windley, B. F., Han, J., Shu, D., Li, Y., 2010. The Ediacaran radiogenic Sr isotope excursion in the Doushantuo Formation in the Three Gorges area, South China. Precambrian Research 176, 46-64.

Shi, W., Li, C., Luo, G., Huang, J., Algeo, T.J., Jin, C., Zhang, Z., Cheng, M., 2018. Sulfur isotope evidence for transient marine-shelf oxidation during the Ediacaran Shuram Excursion. Geology 46, 267-270.

Shields, G., Mills, B., Zhu, M., Raub, T., Daines, S., Lenton, T., 2019. Unique Neoproterozoic carbon isotope excursions sustained by coupled evaporite dissolution and pyrite burial. Nature Geoscience. 12, 823-827.

Stirling, C.H., Andersen, M.B., Potter, E.-K., Halliday, A.N., 2007. Low-temperature isotopic fractionation of uranium. Earth and Planetary Science Letters 264, 208-225.Sui, Y., Huang, C., Zhang, R., Wang, Z., Ogg, J., Kemp, D.B., 2018. Astronomical time scale for the lower Doushantuo Formation of early Ediacaran, South China. Science Bulletin 63, 1485-1494.

Turner, E.C., Bekker, A., 2016. Thick sulfate evaporite accumulations marking a mid-Neoproterozoic oxygenation event (Ten Stone Formation, Northwest Territories, Canada). Geological Society of America Bulletin 128, 203–222.

Tostevin, R. and Mills, B. J. W., 2020. Reconciling proxy records and models of Earth's oxygenation during the Neoproterozoic and Palaeozoic. Interface Focus 10 4 20190137

Van Cappellen, P. Ingall, E. D. , 1994. Benthic phosphorus regeneration, net primary production, and ocean anoxia: A model of the coupled marine biogeochemical cycles of carbon and phosphorus. Paleoceanography 9, 677-692.

Wei, G., Planavsky, N. J., Tarhan, L. G., Chen, X., Wei, W., Li, D., Ling, H., 2018. Marine redox fluctuation as a potential trigger for the Cambrian explosion. Geology 46, 587-590.

Williams, J.J., Mills, B.J.W., Lenton, T.M., 2019. A tectonically driven Ediacaran oxygenation event. Nature Communications 10, 2690.

Wood, R., Liu, A.G., Bowyer, F., Wilby, P.R., Dunn, F.S., Kenchington, C.G., Cuthill, J.F.H., Mitchell, E.G., Penny, A., 2019. Integrated records of environmental change and evolution challenge the Cambrian Explosion. Nature Ecology and Evolution 3, 528-538.

Wortmann, U.G., Paytan, A., 2012. Rapid Variability of Seawater Chemistry Over the Past 130 Million Years. Science 337, 334-336.

Xiao, S., Zhang, Y., Knoll, A.H., 1998. Three-dimensional preservation of algae and animal embryos in a Neoproterozoic phosphorite. Nature 391, 553.

Yuan, X., Chen, Z., Xiao, S., Zhou, C., Hua, H., 2011. An early Ediacaran assemblage of macroscopic and morphologically differentiated eukaryotes. Nature 470, 390.

Zhang, F., Romaniello, S. J., Algeo, T. J., Lau, K. V., Clapham, M. E., Richoz, S., Herrmann, A. D., Smith, H., Horacek, M., Anbar, A. D., 2018. Multiple episodes of extensive marine anoxia linked to global warming and continental weathering following the latest Permian mass extinction. Science advances 4, e1602921,.

Zhang, F., Xiao, S., Romaniello, S. J., Hardisty, D., Li, C., Melezhik, V., Pokrovsky, B., Cheng, M., Shi, W.,Lenton, T. M.,Anbar, A. D., 2019. Global marine redox changes drove the rise and fall of the Ediacara biota. Geobiology 17, 594-610,

Zhou, C., Yuan, X., Xiao, S., Chen, Z., Hua, H., 2018. Ediacaran integrative stratigraphy and timescale of China. Science China Earth Sciences 62, 7-24.

Zhou, C., Li, X., Xiao, S., Lan, Z., Ouyang, Q., Guan, C., Chen, Z., 2017. A new SIMS zircon U–Pb date from the Ediacaran Doushantuo Formation: age constraint on the Weng'an biota. Geological Magazine 154, 1193-1201

Zhu, M., Zhang, J., Yang, A., 2007. Integrated Ediacaran (Sinian) chronostratigraphy of South China. Palaeogeography, Palaeoclimatology, Palaeoecology 254, 7-61.

Zhu, M., Lu, M., Zhang, J., Zhao, F., Li, G., Yang, A., Zhao, X., Zhao, M., 2013. Carbon isotope chemostratigraphy and sedimentary facies evolution of the Ediacaran Doushantuo Formation in western Hubei, South China. Precambrian Research 225, 7-28.

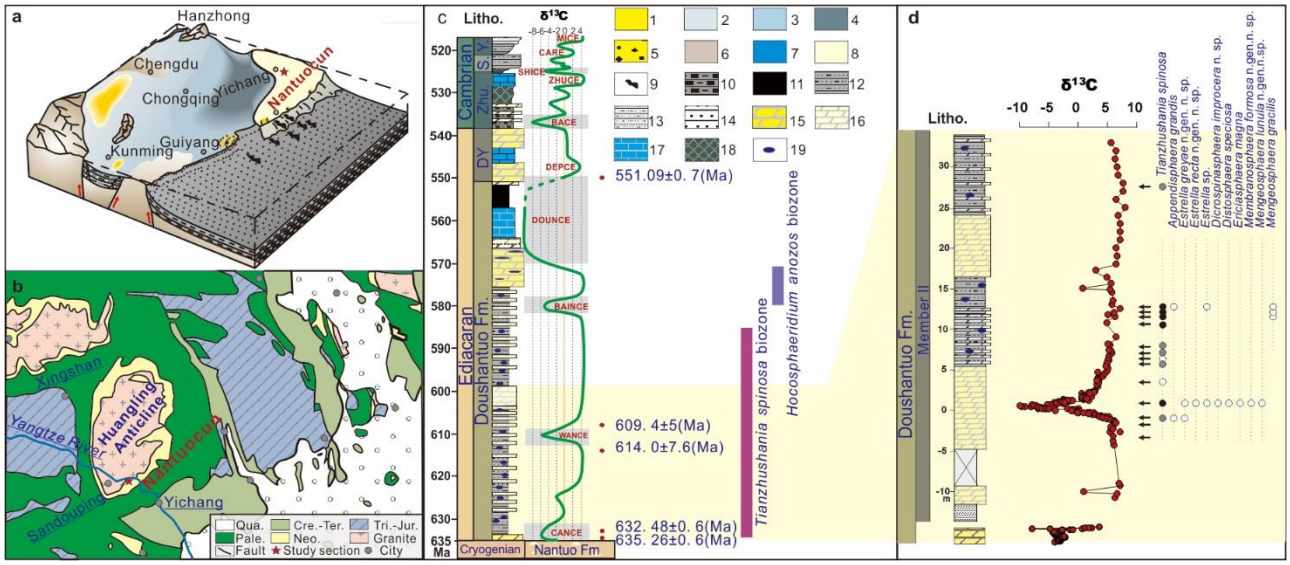

Fig. 1 Geological setting and stratigraphy of the Nantuocun section, Yichang, western Hubei, South China. a. Paleogeographical and b. geological map showing the location of the Nantuocun Section. Qua. = Quaternary, Cre. -Ter. = Cretaceous-Tertiary, Tri. -Jur. = Triassic-Jurassic, Pale. = Paleozoic, Neo. = Neoproterozoic. CANCE = Cap carbonate Negative Carbon isotope Excursion, WANCE = Weng'An Negative Carbon isotope Excursion, BAINCE= Baiguoyuan Negative Carbon isotope Excursion, DOUNCE = Doushantuo Negative Carbon isotope Excursion. DEPCE = Dengying Positive Carbon isotope Excursion, BACE = Basal Cambrian Carbon isotope Excursion ZHUCE = Zhujiaqing Carbon isotope Excursion, SHICE= Shiyantou Carbon isotope Excursion CARC= Cambrian Arthropod Radiation isotope Excursion, MICE = Mingxinsi Carbon Isotope Excursion, c. The generalized litho- and $\delta^{13}C_{carb}$ stratigraphy of the Ediacaran and early Cambrian of the South China(Zhu et al., 2013), and

available radiometric and biostratigraphic data for the Doushantuo Formation(Condon et al., 2005; Zhou et al., 2017) DY = Dengying, Zhu. = Zhujiajing, S. = Shiyantou, Y. =Yuanshan, FM. =Formation. d. Litho-, bio- and $\delta^{13}C_{carb}$ stratigraphy of the Nantuocun section. Yellow shadow showing stratigraphic correlation of the Nantuocun section within the Doushantuo Formation. Legends for c and d: 1. Inter-carbonate platform restricted basin; 2. Coarse clastic basin; 3. Fine clastic basin; 4. Deep water silt and shales basin; 5. Shoal in carbonate platform; 6. Landmass; 7. Inter-carbonate platform deep water basin; 8. Carbonate platform; 9. Slumps; 10. Siliceous rock; 11. Black shale; 12. Black silty shale; 13. Silty shale; 14. Sandstone; 15. Cap carbonate; 16. Dolostone; 17. Limestone; 18. Phosphorite; 19. Cherty concretions.

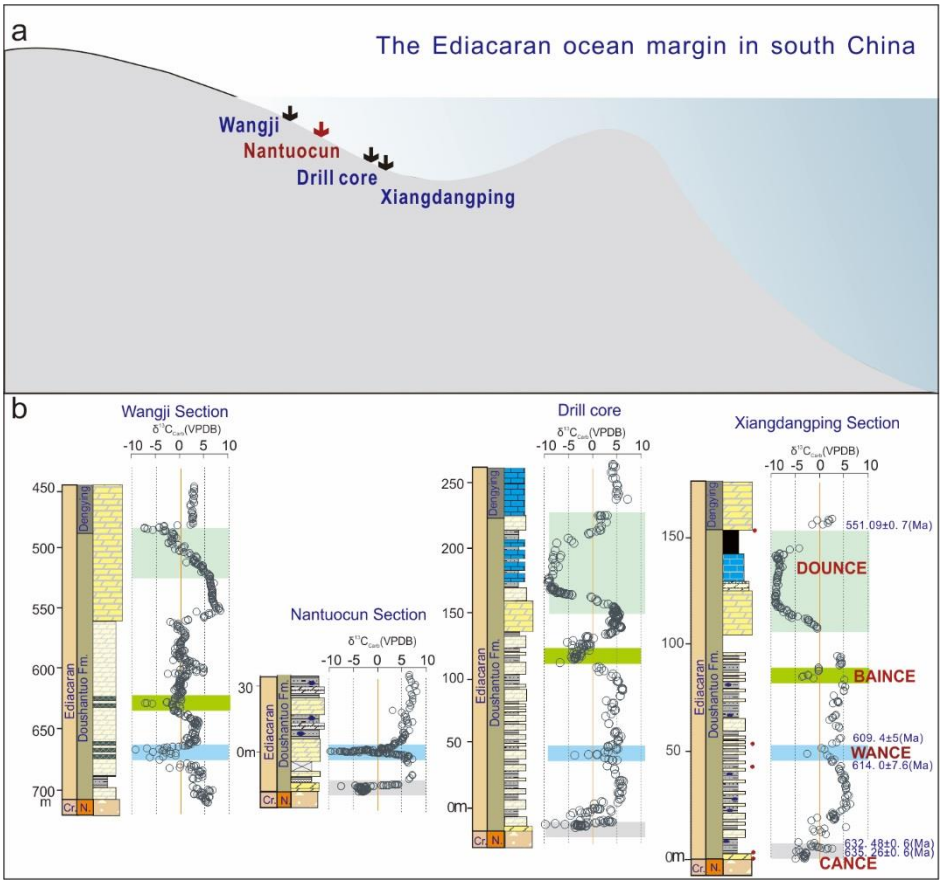

Fig. 2 Palaeogeographic reconstruction of the shelf-to-basin transect showing the wide occurance of WANCE in the Yangtze Gorges area. Legends in b see Fig. 1 data for

Xidangdangping section from Zhu et al. (2013), Drill cole Sawaki et al. (2010), Wangji section Gao et al. (2018).

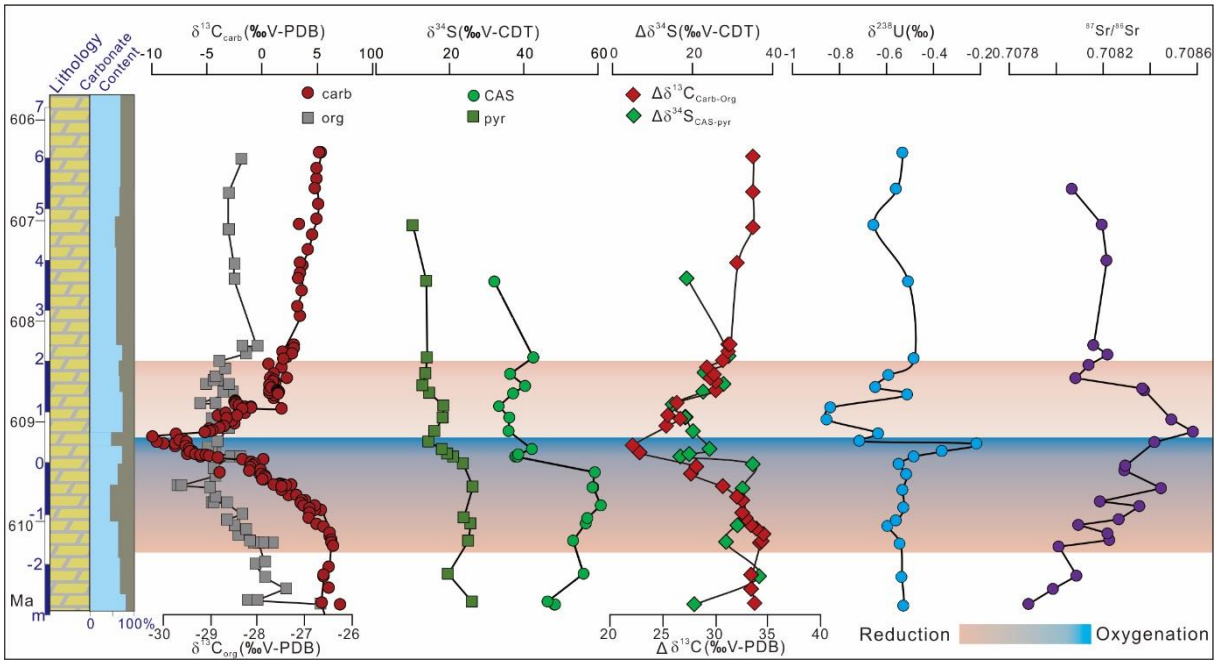

Fig. 3 Paired profiles of inorganic ($\delta^{13}C_{carb}$) and organic carbon ($\delta^{13}C_{org}$) , and pyrite ($\delta^{34}S_{pyr}$) and carbonate associated sulfate ($\delta^{34}S_{CAS}$) isotopes, and $\Delta^{13}C_{carb}$, $\Delta^{34}S$, $\delta^{238}U$ and $^{87}Sr/^{86}Sr$ records for the early Ediacaran WANCE event at the Nantuocun section, South China. See Supplementary Information for stratigraphic details. Carbon and sulfur isotope data are reported relative to Vienna Pee Dee Belemnite (VPDB) and Vienna Cañon Diablo Troilite (VCDT), respectively. $\Delta^{13}C = \delta^{13}C_{carb} - \delta^{13}C_{org}$ and $\Delta^{34}S = \delta^{34}S_{CAS} - \delta^{34}S_{pyr}$. $\delta^{238}U$ is reported relative to the NBL CRM-145 natural U standard.

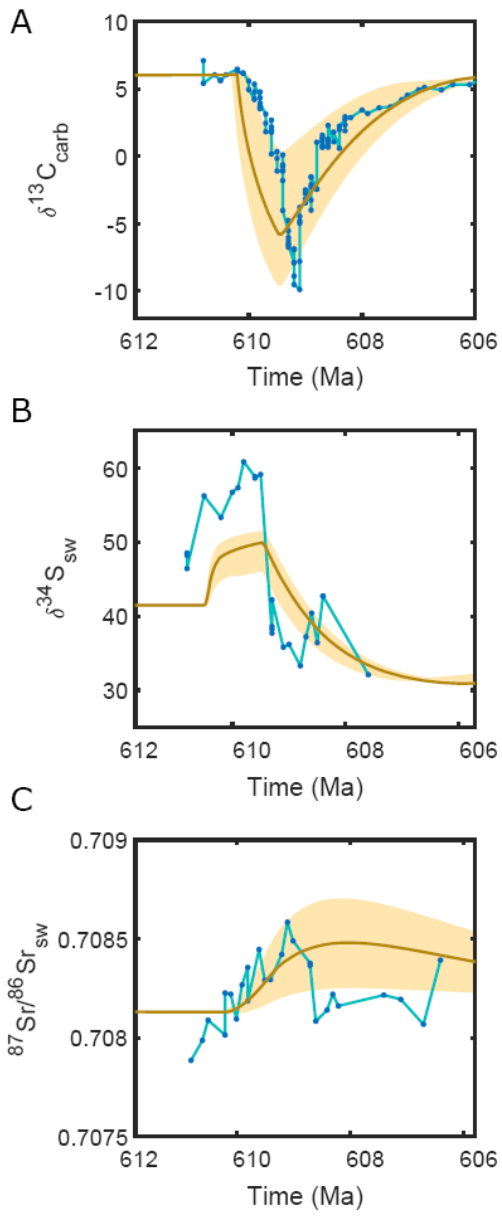

606
607

608 **Fig. 4. COPSE model output against measured isotope ratios.** The most recent COPSE
609 model version (Tostevin and Mills, 2020) is run through the Ediacaran period, with the
610 inclusion of a large reservoir of DOM, following the model approach in Shields et al. (2019).
611 The model is subjected to a stepwise increase in gypsum-derived sulfate input from weathering
612 between 610.5 Ma and 609.5 Ma. The input of pyrite-derived sulfate is also increased at the
613 same time, but remains elevated throughout the model run, reflecting the different weathering
614 dynamics. A. $\delta^{13}C$ of marine carbonate. B. $\delta^{34}S$ of seawater sulfate. C. $^{87}Sr/^{86}Sr$ of seawater.
615 Yellow shading shows model output under 5-15 fold enhancements in gypsum weathering, with
616 the central line showing a 10-fold enhancement. Blue dots show measured datapoints.

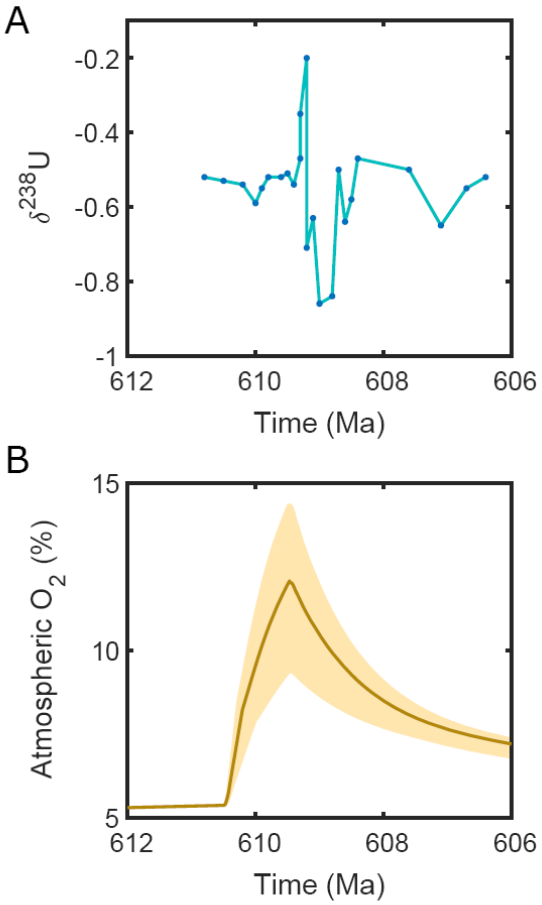

Fig. 5. COPSE model output for oxygenation. A. $\delta^{238}U$ values reported as a function of time. B. Model outputs for the size of the combined atmosphere-ocean O_2 reservoir. Yellow shading shows model output under 5-15 fold enhancements in gypsum weathering, with the central line showing a 10-fold enhancement. Blue dots show measured datapoints.

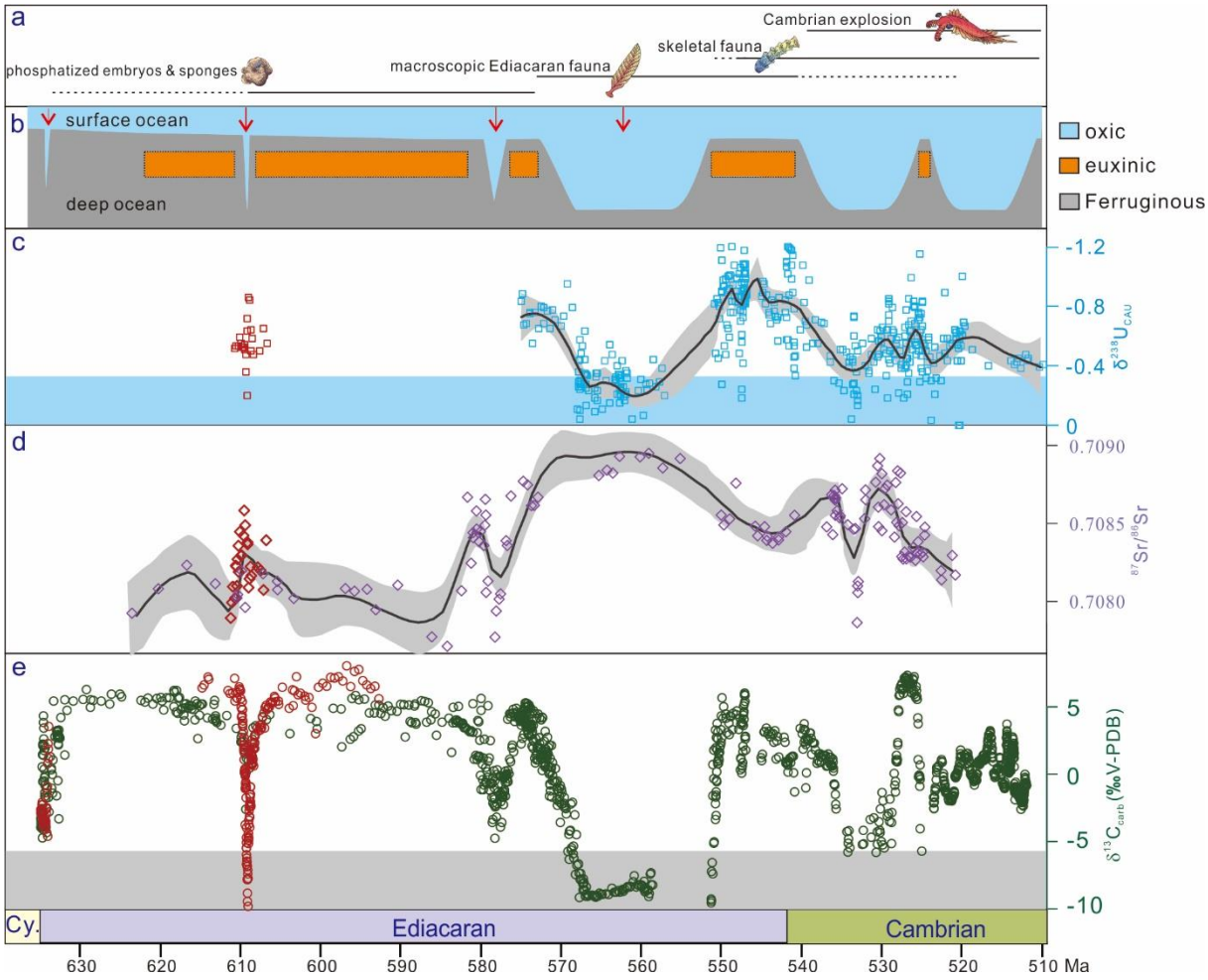

Fig. 6. Integrated key metazoan innovations and ocean oxygenation patterns, and their correlation to marine uranium, strontium and carbon isotopic records, for the Ediacaran and early Cambrian Period. a. The timeline of key evolutionary innovations for metazoans. b. Oxygenation pattern for the Ediacaran and early Cambrian oceans based on this study. c. Uranium isotope record (red squares, this study; blue squares from(Zhang et al., 2018; 2019; Wei et al., 2018; Dahl et al., 2019) and blue shading represent the values above the modern ocean. d. Strontium isotope record (red diamonds, this study; dark blue diamonds from (Sawaki 2010; Maloof, et al., 2010; Li et al., 2013). e. Carbon isotope record (red circles, this study; green circles from (Lu et al., 2013; He et al ., 2019; Li et al., 2013) for the Ediacaran and early Cambrian, grey shading represents values below that of mantle input. Black lines with grey shading in (c) and (d) represent a Locfit regression with 95% confidence interval.

Acknowledgements This work was supported by the Strategic Priority Research Program (B) of the Chinese Academy of Sciences (XDB18000000) and National Natural Science Foundation of China (41661134048) to M.Z., NERC (NE/S009663/1) to B.J.W.M. and S.W.P., the NERC-NSFC programme 'Biosphere Evolution, Transitions and Resilience' through grant NE/P013643/1 to G.A.S. and S.W.P., NERC (N018559/1) to R.J.N. and S.W.P., and the State Key Laboratory of Palaeobiology and Stratigraphy, Chinese Academy of Sciences (No. 20172101; No.2018KF03) to B. C. and T.H., S.W.P. additionally acknowledges support from a Royal Society Wolfson Research Merit Award. We acknowledge Tian Chao for assistance with figure preparation and Li Guang and S. Reid for assistance in the field work and geochemical analyses.